Perfect quantum transport in arbitrary spin networks

Ashok Ajoy and Paola Cappellaro

Phys. Rev. B **87**, 064303 — Published 25 February 2013

DOI: 10.1103/PhysRevB.87.064303

Perfect quantum transport in arbitrary spin networks

Ashok Ajoy and Paola Cappellaro*
Department of Nuclear Science and Engineering and Research Laboratory of Electronics, Massachusetts Institute of Technology, Cambridge, MA, USA

Spin chains have been proposed as wires to transport information between distributed registers in a quantum information processor. Unfortunately, the challenges in manufacturing linear chains with engineered couplings has hindered experimental implementations. Here we present strategies to achieve perfect quantum information transport in arbitrary spin networks. Our proposal is based on the weak coupling limit for pure state transport, where information is transferred between two end-spins that are only weakly coupled to the rest of the network. This regime allows disregarding the complex, internal dynamics of the bulk network and relying on virtual transitions or on the coupling to a single bulk eigenmode. We further introduce control methods capable of tuning the transport process and achieve perfect fidelity with limited resources, involving only manipulation of the end-qubits. These strategies could be thus applied not only to engineered systems with relaxed fabrication precision, but also to naturally occurring networks; specifically, we discuss the practical implementation of quantum state transfer between two separated nitrogen vacancy (NV) centers through a network of nitrogen substitutional impurities.

PACS numbers: 03.67.Ac, 03.67.Hk

I. INTRODUCTION

Transport of quantum information between distant qubits is an essential task for quantum communication[1] and quantum computation[2]. Linear spin chains have been proposed[3] as quantum wires to connect distant computational units of a distributed quantum processor. This architecture would overcome the lack of local addressability of naturally occurring spin networks by separating in space the computational qubit registers while relying on free evolution of the spin wires to transmit information among them. Engineering the coupling between spins can improve the transport fidelity[4], even allowing for *perfect* quantum state transport (QST), but it is difficult to achieve in experimental systems. Remarkable work[5,6] found relaxed coupling engineering requirements – however, even these proposals still required linear chains with nearest-neighbor couplings[7,8] or networks will all equal couplings[9]. These requirements remain too restrictive to allow an experimental implementation, since manufacturing highly regular networks is challenging with current technology[10–13].

Here we describe strategies for achieving QST between separated "end"-spins in an *arbitrary* network topology. This allows the use of natural spin networks (e.g. in crystals) with almost no fabrication requirements. In large networks, the end-spins are intrinsincally weakly coupled to the bulk network, allowing the use of a perturbative approach to describe the transport dynamics in this weak-coupling regime[5–9,14]. We identify two different scenarios for engineering perfect transport: the end-spins could be set far off-resonance from the rest of the network – transport is then driven by a second-order process and hence is slow, but it requires no active control. Alternately, faster transport is achievable by bringing the end-spins in resonance with a mode of the bulk of the network, effectively creating a Λ-type network[15], whose dynamics and bandwidth we characterize completely. We further introduce a simple control sequence that ensures perfect QST by properly *balancing* the coupling of the end-spins to the common bulk mode, thus allowing perfect and fast state transfer. Finally, we investigate the scaling of QST in various types of networks and discuss practical implementations for QST between separated nitrogen vacancy (NV) centers in diamond[16,17] via randomly positioned electronic Nitrogen impurities[18–21].

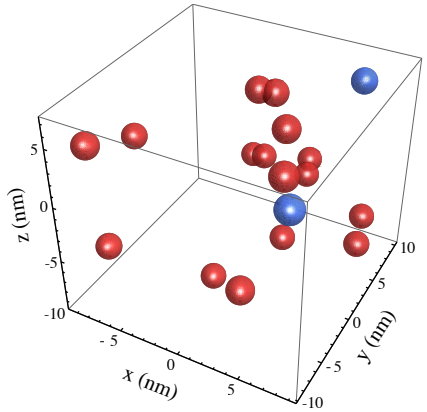

FIG. 1. Example of spin network, consisting of NV centers (blue spheres) and P1 centers (red) in a diamond lattice. The network is given by randomly positioned P1 centers in the diamond lattice with a concentration of 0.2 ppm and a 5% conversion efficiency to NV. The proposed strategies enable perfect quantum state transfer between the two NV spins in this naturally occurring topology of P1 centers[20,21].

II. SPIN NETWORK

The system (Fig. 1) is an N-spin network, whose nodes represent spins-$\frac{1}{2}$ and whose edges H_{ij} are the Hamiltonian coupling spins i and j. We consider the isotropic XY Hamiltonian, $H_{ij} = (S_i^+ S_j^- + S_i^- S_j^+)$, with $S_j^\pm = \frac{1}{2}(S_j^x \pm i S_j^y)$, which has been widely studied for quantum transport[3,15,22,23]. We further assume that two nodes, labeled 1 and N, can be partially controlled and read out, independently from the *bulk* of the network: we will consider QST between these *end* spins. For perfect transport, an excitation created at the location of spin 1 should be transmitted without distortion to the position of spin N upon evolution under H. We characterize the efficiency of transport by the fidelity, $F(t) = |\langle N| e^{-iHt} |1\rangle|^2$, where $|j\rangle$ represents a single excitation $|1\rangle$ at spin j, while all other spins are in the ground state $|0\rangle$.

III. WEAK-COUPLING REGIME

The system Hamiltonian can be subdivided into a part, H_B, that describes the couplings in the bulk network, and a part, H_e, that contains the couplings of the end-spins to the bulk. While optimal fidelity has been obtained for specific, engineered networks (mainly 1D, nearest-neighbor chains), here we consider a completely arbitrary bulk network H_B. To ensure perfect transport, we work in the weak-coupling regime for the end-spin coupling H_e. We set the total Hamiltonian to

$$H = \boldsymbol{\beta} H_B + \epsilon H_e, \tag{1}$$

where we impose $\epsilon \|H_e\| \ll \boldsymbol{\beta} \|H_B\|$, by engineering appropriate weights $\epsilon, \boldsymbol{\beta}$. (Here $\|\cdot\|$ is a suitable matrix norm[24]).

Intuitively, we expect the weak coupling regime to achieve perfect transfer since it imposes two rates to the spin dynamics: the bulk spins evolve on a "fast" time scale while the end-spin dynamics is "slow". The end spins inject information into the network bulk, which evolves so quickly that information spreads everywhere at a rate much faster than new information is fed in, allowing an adiabatic elimination[28] of the information quantum walk in the bulk network[15]. Although high fidelity can be reached, this *off-resonance* transport is slow.

A different strategy for information transport, and a faster rate, is achieved by bringing the end-spins *on resonance* with an eigenmode of the bulk – the weak coupling ensuring greater overlap with a single (possibly degenerate) mode. The system reduces to a Λ-network[15], where coupled-mode theory ensures perfect transport if both ends have equal overlaps with the bulk mode[29,30], a condition that we will show can be engineered by the control sequence in Fig. 2.

To make more rigorous our intuition of the weak regime, we describe transport via a perturbative treatment. Transport in the single excitation subspace is fully described by the adjacency matrix A[4], defined via $H = \sum_{i<j} A_{ij}(S_i^+ S_j^- + h.c.)$. For convenience we consider normalized matrices, $\|H_B\| = \|H_e\| = 1$, and introduce the network adjacency matrix, $A = \boldsymbol{\beta} A^B + \epsilon A^e$, which describes the coupling networks of the system Hamiltonian Eq. (1); in the weak-coupling regime $\gamma = \boldsymbol{\beta}/\epsilon \gg 1$.

The fidelity can then be written as $F(t) = |\langle N| e^{-iAt} |1\rangle|^2$, where the vectors $|j\rangle$ now represent the node basis in the $N \times N$ network space. We use a Schrieffer-Wolff transformation[31–33] and its truncation to first order in $1/\gamma$ to define an effective adjacency matrix, $A' = e^S A e^{-S} \approx A + \frac{1}{2}[S, A]$, which drives the evolution. Setting S so that $[A^B, S] = \frac{\epsilon}{\boldsymbol{\beta}} A^e$, we have $A' \approx \boldsymbol{\beta} A^B + \frac{\epsilon}{2} A^S$, where $A^S = [S, A^e]$ can be evaluated explicitly.

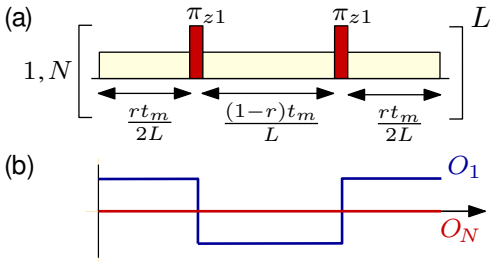

FIG. 2. (a) On-resonance balancing sequence applied to the end spins for perfect quantum transport. Yellow blocks indicate microwave irradiation that brings the end spins on resonance with the bulk network. The resulting Λ-network is in general unbalanced, but appropriately placed π-pulses (orange) on the end-spin with higher mode overlap (here spin 1) can balance the overlaps $O_{(1,N)}$[25]. (b) The π-pulses invert the sign of the coupling of spin at node 1 to the bulk mode in the toggling frame such that $O_{1,N}$ become equal on average. For the network of Fig. 1, $|O_1| > |O_N|$ and $r = 1/2(1 + |O_N/O_1|) = 0.5501$. The sequence is symmetrized[26,27] and repeated for L cycles.

A. Off-resonance QST

Consider first the case where the eigenvalues $\{E_j^B\}$ of A^B are non-degenerate, except for $E_1^B = E_N^B = 0$ (associated with the end-spin subspace). We can fix the energy eigenbasis $\{|v_k\rangle\}$ of A^B by setting $|v_1\rangle = |1\rangle$ and $|v_N\rangle = |N\rangle$. In this basis the structure of the matrix A^e is preserved, non-zero terms connecting only the end-nodes to the bulk, $A^e_{\ell j} = 0$ for $\ell \neq 1, N$. A general element of A^S can be written as

$$A^S_{ij} = \frac{\epsilon^2}{\boldsymbol{\beta}} \sum_k A^e_{ik} A^e_{kj} \left(\frac{1}{E_i^B - E_k^B} + \frac{1}{E_j^B - E_k^B} \right). \tag{2}$$

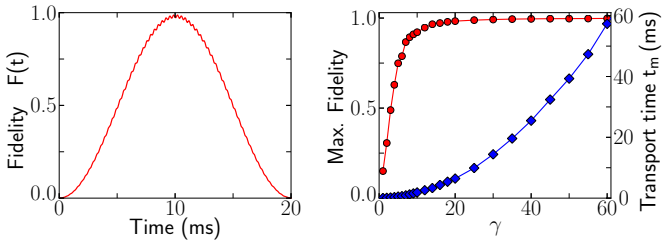

FIG. 3. (a) Off-resonance transport fidelity for the network in Fig. 1 for $\gamma = 25$. Perfect transport occurs, but on a slow time scale, an order of magnitude longer than the on-resonance balanced case (Fig. 4). (b) Increasing γ improves transport fidelity (red circles) but also increases the time required for perfect transport (blue diamonds).

Setting $\{i,j\} \neq 1, N$ and $\{\zeta,\xi\} \in \{1,N\}$, we have

$$A^S_{ij} = \frac{\epsilon^2}{\boldsymbol{\beta}}(A_{i1}A_{1j} + A_{iN}A_{Nj})\left(\frac{1}{E^B_i} + \frac{1}{E^B_j}\right) \quad (3)$$

and

$$A^S_{\zeta\xi} = -\frac{2\epsilon^2}{\boldsymbol{\beta}} \sum_{j\neq 1,N} A^e_{\zeta j}A^e_{j\xi}/E^B_j, \quad (4)$$

while elements between the end- and bulk-nodes are zero, $A^S_{\zeta j} = 0$, if $A^e_{\xi\zeta} = 0$. Hence A^S can be partitioned into a term with support only in the bulk subspace (Eq. 3) and a second term with support only in the end-spin subspace (Eq. 4). To first order approximation, it is only this last term that drives QST – the transport happens via a direct coupling between the end-nodes. Since this effective coupling is mediated by the bulk via virtual transitions, its rate is proportional to $\epsilon^2/\boldsymbol{\beta}$. The fidelity of transport is determined entirely by the effective detuning of the two end-spins, $\alpha = (A^S_{11} - A^S_{NN})/2$:

$$F(t) = \frac{(A^S_{1N})^2}{(A^S_{1N})^2 + \alpha^2} \sin^2\left(t\sqrt{(A^S_{1N})^2 + \alpha^2}\right) \quad (5)$$

If we can modify the end-spin Hamiltonian by adding a term $H_{\text{off}} = -2(\omega_1 S^z_1 + \omega_N S^z_N)$, such that $A^S_{11} + \omega_1 = A^S_{NN} + \omega_N$, perfect quantum transport is ensured at $t_m = \pi/(2A^S_{1N})$. This energy shift could be obtained by locally tuning the magnetic field or by applying local AC driving to the end spins, which ensures they have the desired energy in the rotating frame (similar to the Hartman-Hahn scheme[34,35]). Transport fidelity also depends on the goodness of the first order approximation, increasing with γ at the cost of longer transport times, as shown in Fig. 3(b).

B. On-resonance QST

Transport can be made faster if the end spins are on resonance with one non-degenerate mode of the bulk, $|v_d\rangle$ (we will consider the degenerate case in Appendix A). Resonance happens if the corresponding eigenvalue is $E^B_d = 0$ or it can be enforced by adding an energy shift to the end spins to set $A^e_{11} = A^e_{NN} = \boldsymbol{\beta}/\epsilon E^B_d$. Transport then occurs at a rate proportional to ϵ, as driven by the adjacency matrix A^d, the projection of A^e in the degenerate subspace:

$$A^d = \langle 1|\, A^e\, |v_d\rangle\, |1\rangle\langle v_d| + \langle N|\, A^e\, |v_d\rangle\, |N\rangle\langle v_d| + h.c.$$

We note that the goodness of this approximation depends on the gap between the selected resonance mode and the other bulk modes. In the node basis, A^d forms an effective Λ-*network*[15] (of general form $A^d = \sum_j (A_{1j} + A_{jN}) + h.c.$), coupling the end-spins with each spin of the bulk:

$$A^d = \sum_j (\delta_{1j}\, |1\rangle\langle j| + \delta_{Nj}\, |N\rangle\langle j| + h.c.), \quad (6)$$

where $\delta_{(1,N)j} = \langle v_d|j\rangle\, \langle (1,N)|\, A^e\, |v_d\rangle$. Note that importantly we have $\delta_{1j}/\delta_{Nj} = \text{cst.}, \forall j$. Transport in such Λ-networks occurs at only four frequencies (see Appendix B), $F(t) = w_0 + \sum_{m=1}^4 w_m \cos(f_m t)$ with Fourier coefficients w_m defined below, and the frequencies,

$$f_{1,2} = 2\sqrt{S^2 \mp \sqrt{S^4 - \Delta^4}}\,;\; f_{3,4} = \sqrt{2(S^2 \mp \Delta^2)}, \quad (7)$$

where,

$$\begin{aligned} S^2 &= \sum_j \frac{1}{2}(\delta^2_{1j} + \delta^2_{jN}) \\ \Delta^4 &= \sum_{j<k} (\delta_{1j}\delta_{kN} - \delta_{jN}\delta_{1k})^2 \\ \delta^2 &= \sum_j \delta_{1j}\delta_{jN} \end{aligned} \quad (8)$$

Physically, $S \sim \|A^d\|$ sets the energy scale of the resonant mode, while Δ quantifies the *relative* detuning between different Λ-paths[15] (see Appendix B) .

The Fourier coefficients w_i are found to be $w_0 = -w_3 = -w_4 = \frac{\delta^4}{4(S^4-\Delta^4)}$, $w_1 = w_2 = w_0/2$, giving the analytical expression for QST in a Λ-network,

$$F(t) = \frac{\delta^4}{S^4 - \Delta^4} \sin^2\left(\sqrt{\frac{S^2+\Delta^2}{2}}t\right) \sin^2\left(\sqrt{\frac{S^2-\Delta^2}{2}}t\right) \quad (9)$$

Perfect QST requires $\Delta = 0$ and $\delta = S$. The first condition entails $\delta_{1j}/\delta_{jN} = \text{cst.}\ \forall j$, which is always satisfied by A^d if the resonant bulk mode is non-degenerate. We note that in this case there are only two distinct frequencies in Eq. (7), which act as signatures of *on-resonance* transport. Thus one could search for a bulk mode experimentally by tuning the end-spin couplings until the appearance of the two frequencies. On the other hand, $\delta = S$ requires a *balanced* network, $\delta_{1j} = \delta_{jN}\ \forall j$. For the reduced adjacency matrix A^d this condition is sat-

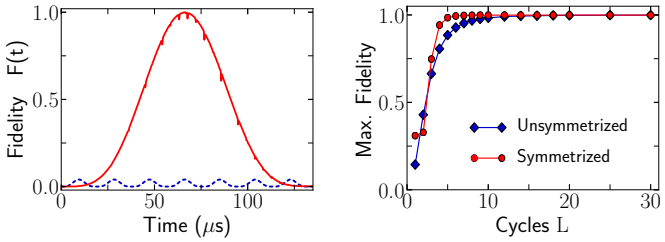

FIG. 4. (a) On-resonance transport fidelity for the network of Fig. 1, with (red) and without (blue, dotted) balancing, for $\gamma = 1$ and $L = 20$. Almost perfect transport occurs in the balanced case, obtained by the control sequence in Fig. 2. (b) Increasing the number of cycles L improves the Trotter approximation yielding enhanced fidelity. The symmetrized sequence performs better than the sequence without symmetrization.

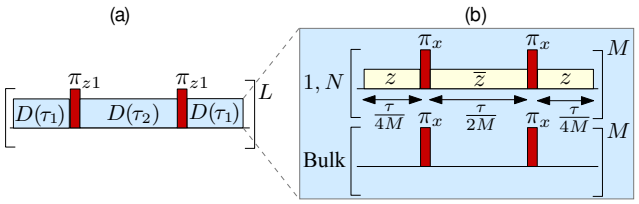

FIG. 5. (a) The control sequence for robust quantum transport under dephasing noise consists of L cycles of a balanced sequence similar to Fig. 2, but constructed out of decoupling blocks $D(\tau)$. Here $\tau_1 = rt_m/2L$ and $\tau_2 = (1-r)t_m/2L$. Panel (b) details the decoupling block $D(\tau)$, consisting of M cycles. The π_x pulses are applied to both the end-spins, and the bulk network. They are accompanied by a toggling of the phase of the microwave irradiation used to bring the end-spins in resonance with the bulk mode. The sequence filters out any dephasing noise field that has a correlation time greater than τ/M; and by appropriately choosing M, the transport can be made immune to noise.

isfied when both end-spins have equal overlap with the resonant eigenmode, $\langle 1|\, A^e\, |v_d\rangle = \langle N|\, A^e\, |v_d\rangle$. In the balanced case the fidelity simplifies to $F(t) = \sin(St/\sqrt{2})^4$, which leads to perfect QST at $t_m = \pi/(\sqrt{2}S)$, as if it were a 3-spin chain[4].

C. Perfect QST by on-resonance balancing

Unfortunately the overlaps of the two end spins with the on-resonance mode, $O_{(1,N)} = \langle (1,N)|A^e|v_d\rangle$, are in general unequal, and the Λ-network unbalanced. Still, it is possible to *balance* the network by a simple control sequence (Fig. 2). Assume without loss of generality $O_1 > O_N$. We partition A^d into effective adjacency matrices with couplings only to spins 1 and N, $A^d = A^d_1 + A^d_N$. A rotation $e^{-iS^z_1\pi}$ on spin 1 produces $\tilde{A}^d = -A^d_1 + A^d_N$. Then, setting $r = \frac{1}{2}(1+|O_N/O_1|)$, the evolution

$$e^{-iA^d rt}e^{-i\tilde{A}^d(1-r)t} \approx e^{-iA^d_b t}, \quad \text{with} \quad A^d_b = A^d r + \tilde{A}^d(1-r),$$

is balanced on *average* during the period t. The approximation improves if one uses L cycles of the control sequence with shorter time intervals (as in a Trotter expansion[27,36]) and appropriately symmetrizes it (see Fig. 2) to achieve an error $\mathcal{O}(r^2(1-r)t^3_m/L^3)$. Fig. 4(a) shows the effect of enhanced, almost perfect, fidelity upon balancing the network of Fig. 1.

Note that for the simplest case of spin chains, the symmetry of the modes ensures the network is already balanced[7,8,37]. However, to drive transport in *arbitrary* networks, one does need an active control scheme for balancing. Similar ideas for engineered mode-matching are employed in the photonics community where the formalism is developed using coupled mode theory[29,30].

IV. REQUIREMENTS FOR PERFECT QST

For transport in real spin networks, the achievable fidelity will be strongly affected by decoherence processes in the spin lattice. It is then necessary to reduce as much as possible the time required for transport. This imposes a compromise between the transport time and the validity of the weak-coupling regime, as they both depend on the weak coupling parameter γ. In addition, constraints in the control achievable may further degrade the fidelity or, conversely, good control on the spin system might improve its coherence properties.

A. Robust transport under decoherence

In many spin systems, the major source of decoherence is dephasing induced by a spin bath[38]. We can be model its effects as a semiclassical dephasing noise field $H_z = \sum_j \omega_j(t) Z_j$, where $\omega_j(t)$ is a stochastic fluctuating field acting on the j^{th} spin. The noise strength $|\langle \omega_j^2 \rangle|$ is roughly proportional to the mean interaction of the spin to its bath, while the correlation time is approximately the inverse of the bath mean spin-spin coupling.

Simple control methods can greatly reduce the effects of dephasing, without affecting the transport Hamiltonian. Consider for instance the control sequence in Fig. 5: A π pulse on the full network takes $H_z \to -H_z$ without changing the coupling Hamiltonian (which is quadratic in the spin operator). If the π-pulses are applied faster than the correlation time of the noise, the noise Hamiltonian is averaged to zero. This decoupling sequence (the decoupling block $D(\tau)$ in Fig. 5) can be embedded in the balancing sequence of Fig. 2. Even more complex control sequences given by various dynamical decoupling schemes[39–42] are compatible with the balancing protocol,

provided we toggle the phase of the continuous irradiation with each π-pulse to maintain the end-spins on resonance with the bulk mode. Dynamical decoupling techniques can thus be used to increase the coherence time[43] to be much longer than the transport time, thus reducing the effects of decoherence on the transport fidelity.

B. Time requirements

We now consider the scaling of the weak coupling parameter γ required for the validity of the perturbative approximation. We can fix $\boldsymbol{\beta} = \|H_B\|$ and consider normalized matrices. Then $\boldsymbol{\beta}$ scales as $\sqrt{(N-2)(N-3)/3}$ for a random network where all the couplings are uniformly distributed. For the more realistic case where the coupling strength decreases with distance, the scaling is less favorable, e.g. for a random dipolar coupled network $\boldsymbol{\beta}$ scales as $\sqrt{2/3(N-3)}/d^3$, where d is the average lattice constant (see Appendix C). Similar scaling occurs for regular spin networks, for example those corresponding to crystal lattices. In general the ratio $\epsilon/\boldsymbol{\beta}$ decreases with the size of the network (usually as $\mathcal{O}(\sqrt{N})$), averting the need to reduce the end-couplings by engineering ϵ, which had been previously deemed necessary[33,37]. For example, $\epsilon = 1$ is sufficient to drive perfect quantum transfer in the network of Fig. 1.

In the case of on-resonance balancing, the time at which perfect QST is achieved is $t_m = \gamma\pi/(\sqrt{2}S)$, where $S = \min\{O_1, O_N\}$ scales linearly with γ. The time is shorter the more symmetrical the end-spins are with respect to the resonant mode, since then $|O_1| \approx |O_N|$. For the off-resonance case the time is $t_m = (\pi\boldsymbol{\beta}/2\epsilon^2)[E^B_\ell/(A^e_{1\ell}A^e_{k\ell})]$, where $E^B_\ell = \min\{|E^B_k|\}$ is the minimum eigenvalue of the bulk. In general this second order transport process takes an order of magnitude longer time than the on-resonance case (Fig. 3).

C. Control requirements

Finally, let us estimate the resources needed to impose the end-spin energy shifts as required for perfect QST, for example by a continuous irradiation during t_m (Fig. 2). In the on-resonance case, the end-spin energy should be set equal to a bulk mode, E^B_d. Selecting the highest bulk eigenmode, which has usually the largest gap to the other modes, E^B_d scales as $\mathcal{O}(N)$ for random networks, but it is constant, $\sim 1.6/d^3$, for dipolar coupled networks (Appendix C). Off-resonance transport requires instead a shift of $A^S_{11} - A^S_{NN}$, where $A^S_{11,NN} = \langle A^e_{1,N}|\ell\rangle^2/\gamma^2 E^B_\ell$, where E^B_ℓ is the minimum bulk eigenmode. Hence the control required in this case is about an order of magnitude lower than in the resonant case.

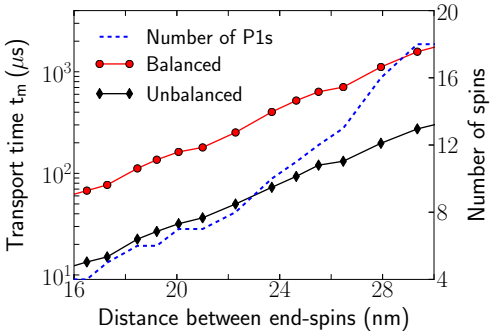

FIG. 6. Time for optimal transport in dipolar coupled spin networks of P1 centers in diamond. The optimal time was calculated from the average over 5000 random lattice realizations of P1 centers of density 10ppm; we considered transport between two NV centers located at increasing distance. The red line (circles) is the time required to achieve a transport fidelity of at least 99% via resonant balancing. The black line (diamonds) is the time at which optimal fidelity is achieved for on-resonant transport without balancing. The fidelity is however quite low ($\sim$15%) in this case. The blue dashed line shows the number of P1 centers in the network, $N-2$.

V. CONCLUSIONS AND OUTLOOK

In this paper, we showed that perfect quantum state transfer can be engineered even in the case of arbitrarily complicated network topologies. The protocols we presented can thus be used to achieve perfect QST even in naturally-occurring, disordered spin systems.

An experimentally important quantum computing architecture is that of nitrogen vacancy (NV) centers in diamond. Fig. 6 shows the scaling of the transport time between two separated NV centers via a bulk network consisting of randomly positioned nitrogen impurities (P1 centers). Transport fidelity loss could occur due to dipolar induced decoherence[44,45]. Dephasing times in excess of 100μs are routinely achievable in diamond[46,47]. Hence from Fig. 6, robust quantum communication is possible in the NV-diamond architecture.

Some experimental challenges remain, although steps to address them have already been taken. In general spins in crystals are coupled by the natural dipolar Hamiltonian and not the isotropic XY Hamiltonian that we assumed here. Thus, we require additional active control to achieve Hamiltonian engineering, for example combining linear gradients with a mixing pulse sequence[21,48–50]. The limitation to pure state transfer requires that the system is polarized at low temperature and high fields. For instance, Ref.[51] demonstrated 99% polarization of a large P1 network ($\sim 10^{16}$ spins) at 2K and 8T. We note that smaller P1 subnetworks could be strongly polarized via the NV centers using cross-polarization[34,52–54].

Thanks to the transport strategies we introduced, many other spin systems can be amenable to act as quantum wires for information transport. Provided the end-spins are detuned off-resonance from the bulk network

(as it would naturally occur in most cases), it is possible to achieve unit transport fidelity with minimal control requirements, although on a somewhat long time scale. Transport speed can be improved by bringing the end-spins on resonance with a common mode of the bulk network. These transport strategies may thus present an alternative to the interlinking of quantum registers with little or no fabrication overhead[55,56]. More generally, the in-depth description of the weak-coupling dynamics for a general network might yield more refined strategies for some specific network topologies.

ACKNOWLEDGMENTS

This work was partially funded by NSF under grant DMG-1005926 and by AFOSR YIP.

Appendix A: Transport for end-spins on-resonance with a degenerate mode

In the main text we described transport when the end spins are on resonance with an eigenmode of the bulk with eigenvalue E_d^B. Here we generalize to the situation where the eigenvalue is degenerate, with eigenvectors $|\alpha_m\rangle$. The projector onto the degenerate eigenspace is then,

$$\begin{aligned} P &= (|1\rangle\langle 1| + |N\rangle\langle N|) + \sum_{m\in M} |\alpha_m\rangle\langle\alpha_m| \\ &\equiv (|1\rangle\langle 1| + |N\rangle\langle N|) + P_M, \end{aligned} \tag{A1}$$

and, to first order, transport is driven by the projection of the adjacency matrix A^e into the this subspace, i.e., $A^d = P^\dagger A^e P$. Now we consider that A^e and A^B have the following forms, where "$\times$" denotes a non-zero element:

$$A^e = \begin{bmatrix} & \times & \times & \times & \times & \\ \times & & & & & \times \\ \times & & & & & \times \\ \times & & & & & \times \\ \times & & & & & \times \\ & \times & \times & \times & \times & \end{bmatrix}; \quad A^B = \begin{bmatrix} & & \times & \times & \times & \\ & \times & & \times & \times & \\ & \times & \times & & \times & \\ & \times & \times & \times & & \\ & & & & & \end{bmatrix}.$$

It follows that

$$\langle 1|A^e|1\rangle = 0\,;\ \langle N|A^e|N\rangle = 0\,;\ \langle\alpha_{m'}|A^e|\alpha_m\rangle = 0, \tag{A2}$$

yielding

$$\begin{aligned} A^d = &\sum_m \langle 1|A^e|\alpha_m\rangle(|1\rangle\langle\alpha_m| + |\alpha_m\rangle\langle 1|) \\ &+ \sum_m \langle N|A^e|\alpha_m\rangle(|N\rangle\langle\alpha_m| + |\alpha_m\rangle\langle N|), \end{aligned} \tag{A3}$$

where we have used the fact that A^e is real, and hence $\langle 1|A^e|\alpha_m\rangle = \langle\alpha_m|A^e|1\rangle$. Let us define the end connection vectors,

$$A^e|1\rangle = |n_1\rangle\ ;\ A^e|N\rangle = |n_N\rangle\,. \tag{A4}$$

Then,

$$\begin{aligned} A^d = &\sum_m \langle n_1|\alpha_m\rangle(|1\rangle\langle\alpha_m| + |\alpha_m\rangle\langle 1|) \\ &+ \sum_m \langle n_N|\alpha_m\rangle(|N\rangle\langle\alpha_m| + |\alpha_m\rangle\langle N|) \\ = &\sum_j\sum_m \langle n_1|\alpha_m\rangle\left(\langle\alpha_m|j\rangle|1\rangle\langle j| + \langle j|\alpha_m\rangle|j\rangle\langle 1|\right) \\ &+ \sum_j\sum_m \langle n_N|\alpha_m\rangle\left(\langle\alpha_m|j\rangle|N\rangle\langle j| + \langle j|\alpha_m\rangle|j\rangle\langle N|\right) \end{aligned}$$

or simplifying,

$$A^d = \sum_j (\delta_{1j}|1\rangle\langle j| + \delta_{jN}|N\rangle\langle j| + h.c.), \tag{A5}$$

where $\delta_{(1,N)j} = \langle n_{(1,N)}|P_M|j\rangle$ is the overlap of the end vector n_1 and the node j in the resonant subspace.

To achieve balanced on-resonance transport we require that $\delta_{1j} = \delta_{jN}$ for all j, which implies that both the end-vectors have equal projections in the resonant subspace,

$$P_M|n_1\rangle = P_M|n_N\rangle\,. \tag{A6}$$

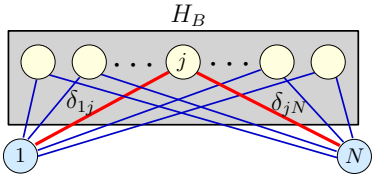

FIG. 7. (Color online) A general detuned Λ-network with multiple Λ-paths between the end spins. Each leg of any of these Λ-paths may have an arbitrary detuning. For the representative case of the Λ-path going through node j (red, thick), these detunings are δ_{1j} and δ_{jN}.

Appendix B: Transport Fidelity for Λ-networks

Here we derive the maximum transport fidelity for a Λ-type network. Λ-type networks are interesting because the effective Hamiltonian of more complex networks reduces to Λ-network Hamiltonian in the weak-coupling regime (as shown in the previous section), but we will consider here the general case.

For any network of adjacency matrix A, the fidelity function $F(t) = |\langle N|\,e^{-iAt}\,|1\rangle|^2$ has a simple expression in the eigenbasis of A,

$$F(t) = \sum_{k,\ell}\langle\ell|N\rangle\langle N|k\rangle\langle k|1\rangle\langle 1|\ell\rangle\cos\left(E_k - E_\ell\right)t. \tag{B1}$$

This shows that the fidelity can be written as the sum

$$F(t) = \sum_n w_n \cos(f_n t), \qquad \text{with} \quad f_n = E_k - E_\ell, \quad \text{(B2)}$$

that is, the frequencies are differences between eigenvalues of A, for which the corresponding eigenvectors $|\ell\rangle$ and $|k\rangle$ have non-zero overlap with $|1\rangle, |N\rangle$.

We now consider a general Λ-network with multiple Λ-paths that connect the end-spins (see Fig. 7) and we will restrict the analysis to the adjacency matrix obtained in the *on-resonance* case only later. We write the adjacency matrix in terms of the coupling strength δ_{1j} and δ_{jN} between the end spin and each j^{th} spin in the bulk, which form the Λ path:

$$A^d = \sum_j \Lambda_j$$
$$\Lambda_j = \delta_{1j}\left(|j\rangle\langle 1| + |1\rangle\langle j|\right) + \delta_{jN}(|j\rangle\langle N| + |N\rangle\langle j|). \quad \text{(B3)}$$

Our strategy for finding the transport fidelity in Λ-networks is to first determine the eigenvalues of the adjacency matrix in Eq. (B3) and hence the possible frequencies at which information transport can occur. Then, we will use a series expansion to find an explicit expression for the fidelity.

1. Frequencies of Transport

The eigenvalues of the adjacency matrix in Eq. (B3) are

$$\begin{aligned} \lambda_0 &= 0, \qquad (N-4) \text{ degenerate} \\ \lambda_{1,2} &= \pm\sqrt{S^2 - \sqrt{S^4 - \Delta^4}}, \\ \lambda_{3,4} &= \pm\sqrt{S^2 + \sqrt{S^4 - \Delta^4}}, \end{aligned} \quad \text{(B4)}$$

where we defined,

$$\begin{aligned} S^2 &= \sum_j S_j^2 = \sum_j \frac{1}{2}(\delta_{1j}^2 + \delta_{jN}^2) \\ \Delta^4 &= \sum_{j<k} \Delta_{jk}^4 = \sum_{j<k} (\delta_{1j}\delta_{kN} - \delta_{jN}\delta_{1k})^2 \\ \delta^2 &= \sum_j \delta_{1j}\delta_{jN} \end{aligned} \quad \text{(B5)}$$

While for a general network the frequencies of transport are differences between the eigenvalues of A^d, here there are only four distinct frequencies because of the symmetries in the eigenvalues:

$$f_0 = 0, \qquad f_1 = 2\lambda_1, \qquad f_2 = 2\lambda_3,$$
$$f_3 = \lambda_1 - \lambda_3 = \sqrt{2(S^2 - \Delta^2)},$$
$$f_4 = \lambda_1 + \lambda_3 = \sqrt{2(S^2 + \Delta^2)}.$$

2. Series expansion

With the frequencies found above, equation Eq. (B2) reduces to $F(t) = \sum_{i=0}^{4} w_i \cos(f_i t)$. To find the parameters w_i, we equate the Taylor expansion of Eq. (B2) and of the fidelity $F(t) = |\langle N| e^{-iAt} |1\rangle|^2$. We only need the first five even power coefficients to fully determine $\{w_i\}$,

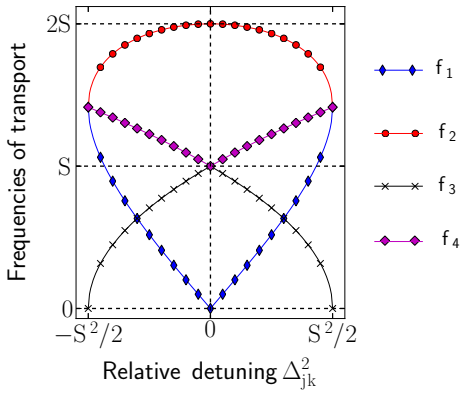

FIG. 8. (Color online) Positive frequencies of transport fidelity for a Λ-network (Fig. 7) consisting of two Λ-paths, $1 \to j \to N$ and $1 \to k \to N$. The frequencies are plotted as a function of the relative detuning between the paths, $\Delta_{jk}^2 = (\delta_{1j}\delta_{kN} - \delta_{jN}\delta_{1k})$. The actual transport also contains symmetric negative frequencies and a DC (zero frequency) component. In general there are four frequencies of transport, derived in Eq. (B6). Note that when δ_{jN}/δ_{1j} is a constant for both paths, there are only two frequencies, S and $2S$, that carry the transport.

giving the series of equations,

$$\begin{aligned}
\sum_{i=0}^{4} w_i &= |\langle N|1\rangle|^2 = 0 \\
\sum_{i=1}^{4} w_i f_i^2 &= -|\langle N|A^d|1\rangle|^2 = 0 \\
\frac{1}{4!}\sum_{i=0}^{4} w_i f_i^4 &= \frac{1}{4}|\langle N|\left(A^d\right)^2|1\rangle|^2 = \mathcal{C}_4 \qquad \text{(B6)} \\
\frac{1}{6!}\sum_{i=0}^{4} w_i f_i^6 &= -\frac{1}{24}\mathrm{Re}[\langle N|\left(A^d\right)^2|1\rangle\langle N|\left(A^d\right)^4|1\rangle] = \mathcal{C}_6 \\
\frac{1}{8!}\sum_{i=0}^{4} w_i f_i^8 &= \frac{1}{4!}|\langle N|\left(A^d\right)^4|1\rangle|^2 \\
&\quad + \frac{1}{2\cdot 6!}\mathrm{Re}[\langle N|\left(A^d\right)^2|1\rangle\langle N|\left(A^d\right)^6|1\rangle] = \mathcal{C}_8
\end{aligned}$$

The expectation values can be evaluated exactly, yielding

$$\begin{aligned}
\mathcal{C}_4 &= \frac{1}{4}\delta^4, \qquad \mathcal{C}_6 = -\frac{1}{12}S^2\delta^4 \qquad \text{(B7)} \\
\mathcal{C}_8 &= \frac{1}{720}\delta^2\left[9S^4 - \Delta^2\right]
\end{aligned}$$

For general frequencies f_i, the coefficients w_i are

$$w_0 = -\sum_{j=1}^{4} w_j; \qquad \text{(B8)}$$

$$w_j = \frac{\mathcal{C}_8 - \sum_{k\neq j} f_k^2\mathcal{C}_6 + \sum_{\ell<m;\ell,m\neq j} f_\ell^2 f_m^2 \mathcal{C}_4}{f_j^2\prod_{k\neq j}(f_k^2 - f_j^2)}, \qquad j > 0$$

Using the expressions for the frequencies in Eq. (B6), we find their explicit expressions in terms of S, Δ and δ:

$$w_0 = \frac{\delta^4}{4(S^4 - \Delta^4)},\ w_1 = w_2 = \frac{w_0}{2},\ w_3 = w_4 = -w_0 \qquad \text{(B9)}$$

The fidelity is thus further simplified to

$$\begin{aligned}
F(t) = \frac{\delta^4}{S^4 - \Delta^4}&\left[\sin\left(t\sqrt{(S^2+\Delta^2)/2}\right)\right. \\
&\left.\times\ \sin\left(t\sqrt{(S^2-\Delta^2)/2}\right)\right]^2 \qquad \text{(B10)}
\end{aligned}$$

3. Fidelity for random and degenerate networks

Consider the case when the number of nodes is large, and the detunings δ_{1j} and δ_{jN} are sampled from the same distribution, as it would be in a random network. Then,

$$\sum_j \delta_{1j}^2 \approx \sum_j \delta_{jN}^2 \qquad \text{(B11)}$$

since the second moments of the random distribution should be equal. In this situation we have

$$S^4 - (\Delta^4 + \delta^4) = \frac{1}{4}\left[\sum_j (\delta_{1j}^2 - \delta_{jN}^2)\right]^2 = 0 \qquad \text{(B12)}$$

Then the condition

$$\delta^4 = S^4 - \Delta^4 \qquad \text{(B13)}$$

is satisfied and the fidelity becomes

$$F(t) = \left[\sin\left(t\sqrt{(S^2+\Delta^2)/2}\right)\sin\left(t\sqrt{(S^2-\Delta^2)/2}\right)\right]^2$$

In the case of resonance to a non-degenerate mode, we have $\Delta = 0$ and the fidelity can reach its maximum $F(t) = \sin(St/\sqrt{2})^4 = 1$, for $t = \pi/\sqrt{2}S$.

For the case of interest in this work, a network where the end-spins are on resonance with a non-degenerate mode, the adjacency matrix of relevance in the weak regime is the reduced adjacency matrix, A^d. As shown above, in this case we have $\Delta = 0$ and the fidelity reduces to

$$F(t) = \left[\frac{\delta}{S}\sin\left(\frac{St}{\sqrt{2}}\right)\right]^4, \qquad \text{(B14)}$$

thus maximum fidelity can be reached only if the condition Eq. (B13) is satisfied. For example, the mirror-symmetric case $\delta_{1j} = \delta_{jN},\ \forall j$ yields the optimal fidelity $F = 1$ since then $\delta = S$.

Appendix C: Estimating matrix norms for different network topologies

1. Different kinds of networks

In this section, we consider different classes of networks, and estimate the norms of the corresponding adjacency matrices A. As described in the main text, the matrix norm of the bulk adjacency matrix is important in predicting the transport time. For example, the scaling of transport time is linear with γ in the on-resonance case; and the value of γ implicitly depends on the norm of the bulk matrix. Hence a large bulk matrix causes an intrinsically high γ, and reduces the control requirements on the end-spins. All the networks considered are of N spins, and hence the adjacency matrices are $N \times N$ matrices.

1. *Random network* – The matrix A has random entries in the range $[0, 1]$ (with appropriate symmetrization). The random entries follow a uniform distribution, with no site-to-site correlation. Overall, this case represents a rather unphysical scenario, but will be useful in the computations that follow.

2. *Random network with $1/d^3$ scaling* – A contains random entries from a uniform distribution scaled by $1/(hd)^3$, where h is the Hamming distance between two nodes. It represents a network similar to a spin chain where all neighbor connectivities are allowed, and there is a possible spread in the position of the nodes from their lattice sites.

3. *Dipolar scaled regular (symmetric) network* – We consider the network to be regular (symmetric) in two and three dimensions. With an appropriate choice of basis, this can be converted to a Bravais lattice. Special cases of interest are the graphene (honeycomb) lattice and the CNT (rolled honeycomb) lattices.

4. *Dipolar scaled regular network with vacancies* – Here we consider the regular network above and introduce vacancies that are binomially distributed with parameter p. This approximately maps to the NV diamond system, where we consider transport through a P1 lattice.

Note that the generalized adjacency matrix A of a network consists of positive numbers in the range $[0, 1]$. This matrix is symmetric and Hermitian.

For the norm, we will use the Frobenius norm, which is the generalized Euclidean norm for matrices.

$$\|A\| = \sqrt{\sum_{i,j}^{N} |a_{ij}|^2} = \sqrt{\sum_{i}^{N} \sigma_i^2} \tag{C1}$$

where σ_i are the singular values of A.

2. Random network

Consider the right triangular form (R-form) of A,

$$A = \begin{bmatrix} 0 & \times & \times & \times & \times & \times \\ & 0 & \times & \times & \times & \times \\ & & 0 & \times & \times & \times \\ & & & 0 & \times & \times \\ & & & & 0 & \times \\ & & & & & 0 \end{bmatrix} \tag{C2}$$

Here $\times$ refers to random numbers uniformly distributed in the range $[0, 1]$. We have $E[X^2] = \mathrm{Var}[X] + (E[X])^2 = 1/12 + 1/4 = 1/3$. The total number of elements in the R matrix is,

$$n = \sum_{j=1}^{N} (N - j) = \frac{N(N-1)}{2} \tag{C3}$$

Hence, since the random numbers are assumed to be uncorrelated from site to site, we have,

$$\|A\| = \sqrt{\frac{N(N-1)}{3}} \tag{C4}$$

Fig. 9(a) shows the linear scaling of the norm in Eq. (C4), compared to the numerically obtained average of 100 manifestations of random networks. The highest eigenvalue of A, $E_{\max}$ also scales linearly with N.

3. Dipolar coupled random network

Now we consider the case where there is $1/d^3$ scaling with the Hamming distance between two nodes. This represents a network similar to a spin chain where all neighbor connectivities are allowed, and there is a possible spread in the position of the nodes from their lattice sites. The adjacency matrix has the form,

$$A = \begin{bmatrix} 0 & \frac{\times}{d^3} & \frac{\times}{(2d)^3} & \frac{\times}{(3d)^3} & \frac{\times}{(4d)^3} & \frac{\times}{(5d)^3} \\ & 0 & \frac{\times}{d^3} & \frac{\times}{(2d)^3} & \frac{\times}{(3d)^3} & \frac{\times}{(4d)^3} \\ & & 0 & \frac{\times}{d^3} & \frac{\times}{(2d)^3} & \frac{\times}{(3d)^3} \\ & & & 0 & \frac{\times}{d^3} & \frac{\times}{(2d)^3} \\ & & & & 0 & \frac{\times}{d^3} \\ & & & & & 0 \end{bmatrix} \tag{C5}$$

As before, assuming that the sites are uncorrelated for the uniform distribution of random numbers $\times$, we have,

$$\begin{aligned} \|A\|^2 &= \frac{2}{3}\left[\frac{N-1}{d^6} + \frac{N-2}{(2d)^6} + \frac{N-3}{(3d)^6} + \cdots + \frac{1}{[(N-1)d]^6}\right] \\ &= \frac{2}{3}\left[\frac{N}{d^6}\sum_{j=1}^{N-1}\frac{1}{j^6} - \frac{1}{d^3}\sum_{j=1}^{N-1}\frac{1}{j^5}\right] \end{aligned} \tag{C6}$$

Consider that,

$$\sum_{j=1}^{N-1}\frac{1}{j^6} \approx \frac{\pi^6}{945} = 1.01734, \ \sum_{j=1}^{N-1}\frac{1}{j^5} \approx 1.036 \tag{C7}$$

and the convergence is very rapid, i.e. it is true even for small N. Then,

$$\|A\| \approx \frac{1}{d^3}\sqrt{\frac{2}{3}(N-1)} \tag{C8}$$

Fig. 9(b) shows that the $\sqrt{N}$ scaling matches very well with the numerically obtained average norm of 100 manifestations of random dipolar networks. The highest eigenvalue $E_{\max}$ approaches a constant $1.6/d^3$.

4. Dipolar coupled regular network

Here we consider a regular, symmetric network in two or three dimensions. To a good approximation, we can assume,

$$\|A\| = n\|A\|_{\mathrm{cell}} \tag{C9}$$

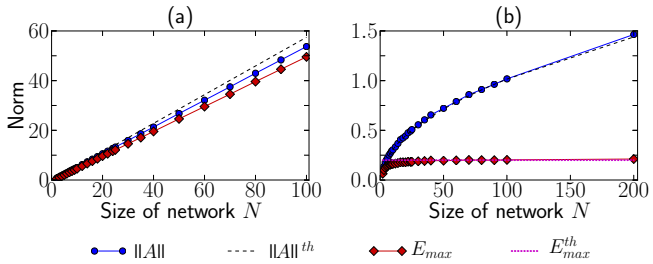

FIG. 9. (Color online) Figure shows the scaling with network size N of the matrix norms and largest eigenmodes of the adjacency matrices corresponding to (a) a random network and (b) a dipolar random network. The solid lines are average values obtained from 100 manifestations of the networks. The dashed lines are theoretical results. For the dipolar network, the largest eigenmode $E_{\max}$ approaches a constant $1.6/d^3$ (dashed magenta line).

where $\|A\|_{\text{cell}}$ is the adjacency matrix of the unit cell of the underlying lattice, and n is the number of tilings of this unit cell,

$$n \approx \frac{N}{N_{\text{cell}}} \tag{C10}$$

where N_{cell} is the number of nodes per unit cell.

$\|A\|_{\text{cell}}$ depends on the choice of lattice in the particular network. Let us consider the case of a honeycomb lattice, where we assume only nearest neighbor interactions. This network is found naturally in graphene and CNTs. Then, $\|A\|_{\text{cell}} = 24/d^3$. Hence, for graphene,

$$\|A\| = \frac{2\sqrt{N}}{d^3} \tag{C11}$$

5. Dipolar coupled regular network with vacancies

Let the probability of a vacancy occurring be p. Once again we assume a binomial distribution. We also assume, that we can estimate the norm in this case by using tiling – i.e. we consider the vacancies only in the unit cells. Consider for simplicity the special case of graphene. For j vacancies, we have,

$$P_j = {}^{N_{\text{cell}}}C_j p^j (1-p)^{N_{\text{cell}}-j} \tag{C12}$$

The corresponding adjacency matrix,

$$\|A\|_j = \frac{4N_{\text{cell}} - j}{d^3} \tag{C13}$$

Hence the mean,

$$\|A\|_{\text{cell}} = \sum_j P_j \|A\|_j = \frac{4N_{\text{cell}}(1-p)}{d^3} \tag{C14}$$

Hence,

$$\|A\| = \frac{2\sqrt{N(1-p)}}{d^3} \tag{C15}$$

* pcappell@mit.edu

[1] H. J. Kimble, Nature **453**, 1023 (2008).
[2] J. I. Cirac, P. Zoller, H. J. Kimble, and H. Mabuchi, Phys. Rev. Lett. **78**, 3221 (1997).
[3] S. Bose, Phys. Rev. Lett. **91**, 207901 (2003).
[4] M. Christandl, N. Datta, A. Ekert, and A. J. Landahl, Phys. Rev. Lett. **92**, 187902 (2004).
[5] A. Wojcik, T. Luczak, P. Kurzynski, A. Grudka, T. Gdala, and M. Bednarska, Phys. Rev. A **72**, 034303 (2005).
[6] Y. Li, T. Shi, B. Chen, Z. Song, and C.-P. Sun, Phys. Rev. A **71**, 022301 (2005).
[7] G. Gualdi, V. Kostak, I. Marzoli, and P. Tombesi, Phys. Rev. A **78**, 022325 (2008).
[8] N. Y. Yao, L. Jiang, A. V. Gorshkov, Z.-X. Gong, A. Zhai, L.-M. Duan, and M. D. Lukin, Phys. Rev. Lett. **106**, 040505 (2011).
[9] A. Wójcik, T. Łuczak, P. Kurzyński, A. Grudka, T. Gdala, and M. Bednarska, Phys. Rev. A **75**, 022330 (2007).
[10] F. W. Strauch and C. J. Williams, Phys. Rev. B **78**, 094516 (2008).
[11] C. F. Hirjibehedin, C. P. Lutz, and A. Heinrich, Science **312**, 1021 (2006).
[12] P. Spinicelli, A. Drau, L. Rondin, F. Silva, J. Achard, S. Xavier, S. Bansropun, T. Debuisschert, S. Pezzagna, J. Meijer, V. Jacques, and J.-F. Roch, New J. Phys. **13**, 025014 (2011).
[13] A. Ajoy, R. K. Rao, A. Kumar, and P. Rungta, Phys. Rev. A **85**, 030303 (2012).
[14] L. Banchi, T. J. G. Apollaro, A. Cuccoli, R. Vaia, and P. Verrucchi, New Journal of Physics **13**, 123006 (2011).
[15] A. Ajoy and P. Cappellaro, Phys. Rev. A **85**, 042305 (2012).
[16] M. V. G. Dutt, L. Childress, L. Jiang, E. Togan, J. Maze, F. Jelezko, A. S. Zibrov, P. R. Hemmer, and M. D. Lukin, Science **316**, 1312 (2007).
[17] F. Jelezko and J. Wrachtrup, Physica Status Solidi (A) **203**, 3207 (2006).
[18] R. C. Barklie and J. Guven, Journal of Physics C: Solid State Physics **14**, 3621 (1981).
[19] R. Hanson, V. V. Dobrovitski, A. E. Feiguin, O. Gywat, and D. D. Awschalom, Science **320**, 352 (2008).
[20] P. Cappellaro, L. Viola, and C. Ramanathan, Phys. Rev. A **83**, 032304 (2011).
[21] N. Yao, L. Jiang, A. Gorshkov, P. Maurer, G. Giedke, J. Cirac, and M. Lukin, Nat Commun **3**, 800 (2012).
[22] P. Cappellaro, C. Ramanathan, and D. G. Cory, Phys. Rev. Lett. **99**, 250506 (2007).
[23] S. C. Benjamin and S. Bose, Phys. Rev. Lett. **90**, 247901 (2003).
[24] R. Bhatia, Matrix Analysis (Springer, 1996).

[25] A. Ajoy, G. A. Álvarez, and D. Suter, Phys. Rev. A **83**, 032303 (2011).
[26] M. H. Levitt, J. Chem. Phys. **128**, 052205 (2008).
[27] M. Suzuki, Phys. Lett. A **146**, 319 (1990).
[28] C. W. Gardiner, Phys. Rev. A **29**, 2814 (1984).
[29] H. Haus and W. Huang, Proceedings of the IEEE **79**, 1505 (1991).
[30] A. Synder and J. Love, Optical Waveguide Theory (Springer, 1983).
[31] J. R. Schrieffer and P. A. Wolff, Phys. Rev. **149**, 491 (1966).
[32] S. Bravyi, D. DiVincenzo, and D. Loss, Ann. Phys. **326**, 2793 (2011).
[33] S. Oh, L.-A. Wu, Y.-P. Shim, J. Fei, M. Friesen, and X. Hu, Phys. Rev. A **84**, 022330 (2011).
[34] S. R. Hartman and E. L. Hahn, Phys. Rev. **128**, 2042 (1962).
[35] A. Pines, M. G. Gibby, and J. S. Waugh, J. Chem. Phys. **59**, 569 (1973).
[36] H. F. Trotter, Proc. Amer. Math. Soc. **10**, 545 (1959).
[37] T. J. G. Apollaro, L. Banchi, A. Cuccoli, R. Vaia, and P. Verrucchi, Phys. Rev. A **85**, 052319 (2012).
[38] L. Cywinski, R. M. Lutchyn, C. P. Nave, and S. DasSarma, Phys. Rev. B **77**, 174509 (2008).
[39] H. Y. Carr and E. M. Purcell, Phys. Rev. **94**, 630 (1954).
[40] S. Meiboom and D. Gill, Rev. Sc. Instr. **29**, 688 (1958).
[41] L. Viola, E. Knill, and S. Lloyd, Phys. Rev. Lett. **82**, 2417 (1999).
[42] G. S. Uhrig, Phys. Rev. Lett. **98**, 100504 (2007).
[43] G. A. Álvarez, A. Ajoy, X. Peng, and D. Suter, Phys. Rev. A **82**, 042306 (2010).
[44] A. Kay, Int. J. of Quantum Info. **8**, 641 (2010).
[45] J.-M. Cai, Z.-W. Zhou, and G.-C. Guo, Phys. Rev. A **74**, 022328 (2006).
[46] P. L. Stanwix, L. M. Pham, J. R. Maze, D. Le Sage, T. K. Yeung, P. Cappellaro, P. R. Hemmer, A. Yacoby, M. D. Lukin, and R. L. Walsworth, Phys. Rev. B **82**, 201201 (2010).
[47] G. Balasubramanian, P. Neumann, D. Twitchen, M. Markham, R. Kolesov, N. Mizuochi, J. Isoya, J. Achard, J. Beck, J. Tissler, V. Jacques, P. R. Hemmer, F. Jelezko, and J. Wrachtrup, Nat Mater **8**, 383 (2009).
[48] L. Braunschweiler and R. Ernst, J. Mag. Res. **53**, 521 (1983).
[49] J. Sleucher, J. Quant, S. J. Glaser, and C.Griesinger, Encyclopedia of Nuclear Magnetic Resonance **6**, 4789 (1996).
[50] G. A. Álvarez, M. Mishkovsky, E. P. Danieli, P. R. Levstein, H. M. Pastawski, and L. Frydman, Phys. Rev. A **81**, 060302 (2010).
[51] S. Takahashi, R. Hanson, J. van Tol, M. S. Sherwin, and D. D. Awschalom, Phys. Rev. Lett. **101**, 047601 (2008).
[52] E. C. Reynhardt and G. L. High, The Journal of Chemical Physics **109**, 4090 (1998).
[53] A. E. Dementyev, D. G. Cory, and C. Ramanathan, Phys. Rev. Lett. **100**, 127601 (2008).
[54] C. Belthangady, N. Bar-Gill, L. Pham, K. Arai, D. Le Sage, P. Cappellaro, and R. Walsworth, arXiv:1211.2749 (2012).
[55] P. Rabl, S. J. Kolkowitz, F. H. L. Koppens, J. G. E. Harris, P. Zoller, and M. D. Lukin, Nat Phys **6**, 602 (2010).
[56] K. Stannigel, P. Rabl, A. S. Sørensen, P. Zoller, and M. D. Lukin, Phys. Rev. Lett. **105**, 220501 (2010).